

Effect of rhenium on defects evolution behavior in tungsten under irradiation

Zheng Wang^{1,2‡}, Liang Gao^{3,4‡}, Xiu-Li Zhu⁵, Yue Yuan^{2,6*}, Shi-Wei Wang^{2,6},
Long Cheng^{2,6}, Guang-Hong Lu^{2,6}

¹ Sino-French Engineer School, Beihang University, Beijing 100191, China

² Beijing Key Laboratory of Advanced Nuclear Materials and Physics, Beihang University, Beijing 100191, China

³ Forschungszentrum Jülich GmbH, Institut für Energie- und Klimaforschung, 52425 Jülich, Germany

⁴ Max-Planck-Institut für Plasmaphysik, Boltzmannstraße 2, D-85748 Garching, Germany

⁵ School of Nuclear Science and Engineering, North China Electric Power University, Beijing 102206, China

⁶ School of Physics, Beihang University, Beijing 100191, China

[‡] Authors with the same contribution to the present work

*E-mail address: yueyuan@buaa.edu.cn

Abstract: The influence of the transmutation element rhenium (Re) on defect evolution in tungsten (W) during irradiations with heavy ions and deuterium (D) plasma was investigated. Rolled W and W-5Re alloy (Re concentration 5 wt.%) were irradiated with 500 keV iron ions to 0.06 and 0.6 dpa (displacement per atom), and deuterium plasma at 38 eV/D to a fluence of 2.2×10^{25} D m⁻² at ~373 K. The results of Doppler broadening spectroscopy by the positron annihilation technique indicate that more or larger vacancy-type defects were produced in W than in the W-5Re during Fe ion irradiation, suggesting the important role of Re on inhibiting the migration and/or clustering of vacancies. The much smaller and shallower blistering in W-5Re than in W after the same D plasma exposure points to the pinning effects on dislocations by Re. The total retained D amounts in W-5Re and W materials are comparable, but with very different concentration profile at corresponding depth. This is explained by the blister formation exerting influence on the D inward diffusion. Demonstrating the

important role of Re on the defect evolution in W under irradiation, the present work provides an enhanced understanding on the possible effects of neutron irradiation on the performance of plasma-facing materials in future fusion devices.

Key words: tungsten, tungsten-rhenium alloy, heavy-ion irradiation, vacancy-type defects, surface blistering, deuterium retention

1. Introduction

Due to its outstanding thermal properties and low hydrogen solubility, tungsten (W) is considered as the most promising plasma-facing material (PFM) for the divertor region in fusion devices [1]. During plasma operations in future fusion devices, W-PFM will be inevitably subjected to extensively high heat and particle fluxes, including neutron, hydrogen isotopes and helium, etc. [2]. The properties of W will be seriously degraded under such extreme irradiation conditions. High-energy neutron irradiation will introduce a large number of vacancies and dislocations; high-flux D/He plasma irradiation may cause blisters or fuzz structures on W surface; transient heat loads can lead to surface cracking or melting [2][3]. Moreover, rhenium (Re) (as well as tantalum, osmium, etc.) will be produced in the W matrix by transmutation under fusion neutron irradiation. It is reported that the Re concentration in W could reach up to 3.8 at. % after five years irradiation [4][5]. Therefore, the influence of Re on the evolution of irradiation-induced defects and on the D/He behavior in W asks for comprehensive understanding.

Due to the extremely low hydrogen solubility, D behaviour in W is dominated by crystal defects acting as trap sites for D, such as impurities, grain boundaries, dislocations, vacancies and so on. On the one hand, alloying elements could affect D behaviours by themselves as impurities. On the other hand, they can affect hydrogen isotope behaviour in W matrix via interacting with crystal defects [6][7]. Grain boundaries and dislocations are commonly accepted as the most probable nucleation sites for inter- and intra-granular cracks, respectively, which lead to surface blistering and in turn exert significant influence on D retention in the bulk below the blister-corresponding cavities [8][9]. Yi et al. [10][11] studied the evolution of irradiation induced dislocation-type defects by TEM observation, and reported that Re alloying can suppress the growth of irradiation defects in W, because Re restricts the mobility of dislocation loops or enhances the recombination between vacancy and interstitial. Lots of studies also revealed that the number density increase of vacancy-type defects caused by displacement damage plays an important role on D retention in W

[12][13][14]. However, due to their small dimensions, vacancy-type defects in irradiated W materials are experimentally very hard to characterize. Hence, there are few studies focusing on the effect of Re on the evolution of vacancy-type defects in W.

Some experimental studies suggested that the effect of Re on D retention in W is strongly correlated with irradiation temperature [15][16]. At room temperature, Re concentration in W–Re alloy does not influence the D retention noticeably [15][16]. At temperatures above 500 K, D retention in W-Re alloys is lower than in pure W. It is explained by the temperature dependence of the ductility of materials, since better ductility prevents blistering on the surface of a W-Re alloy [16]. Computational methods were also used to investigate the influence of Re on D behavior in W. For example, Ma et al. [17] reported that the vacancy trapping capability for H is weakened due to the Re aggregation around vacancies, and this weakening effect will increase with the number of aggregated Re atoms.

In the present work, the influence of Re addition on the evolution of irradiation defects in W was investigated. Specifically, the effect of Re on the vacancy-type defects evolution in W during heavy-ion irradiation was studied by using positron annihilation technique. The Re influence on dislocations and grain boundaries was investigated via a detailed study of the blistering morphology and the correlated D retention in samples after D plasma exposure. Such post-plasma-exposure studies turned out to be effective tools to reveal the influence of Re on defects evolution and fuel retention of W in future fusion devices.

2. Experimental details

W and W-Re alloy (with Re concentration of 5 wt.%) were fabricated by hot rolling process. Both of them have a relative density of >99.5%. Samples with dimensions of $5\times 5\times 1$ mm³ were mechanically polished to a mirror-like finish. Vacuum annealing was performed at 1273 K for 2 hours in order to outgas and release the surface residual stress. Surface morphology of the pristine W and W–Re alloy are shown in Fig. 1. Although surface distortions induced by mechanical polishing remain in some grains

as different grayscale shadings, they should be mostly annealed during the heating treatment. The average crystal grain size of both materials can be determined to be in the order of 1 μm .

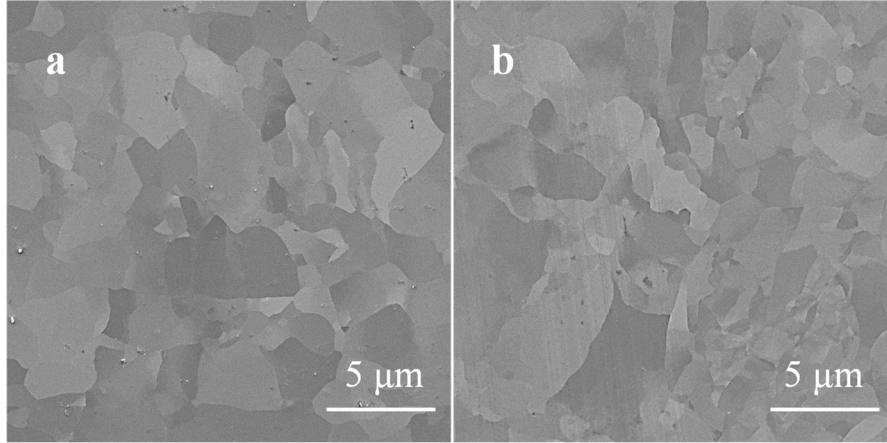


Fig. 1 Surface morphology of the pristine W (a) and W-Re alloy (b).

W and W-Re alloy samples were damaged by 0.5 MeV Fe^{10+} ions on the 320 kV platform of Heavy Ion Research Facility in Lanzhou (HIRFL), China [18]. Fe^{10+} ions were accelerated through a potential difference of 50 kV. The applied ion flux was 3.65×10^{15} ion $\text{m}^{-2} \text{s}^{-1}$, and total fluences were 3.87×10^{17} ion m^{-2} and 3.87×10^{18} ion m^{-2} for 0.06 and 0.6 dpa damage, respectively. During the irradiation, surface temperature of all samples was kept at around room temperature by a water-cooling system. Damage level in dpa (displacements per atom) is calculated applying $\text{dpa} = N_d \Phi / N_w$, where N_d is the number of displacements, which can be calculated by TRIM simulation (SRIM 2008). Φ is the irradiation fluence (ion m^{-2}), and N_w is the atomic density of tungsten (6.338×10^{28} atom m^{-3}) [19].

In the SRIM program, the displacement threshold energy (E_d) was set as 90 eV [20] and ‘Ion distribution and quick calculation of damage’ option was ticked. The calculated damage level and Fe concentration in W is increased proportionally with the ion fluence. Peak damage levels of 0.06 dpa and 0.6 dpa can be obtained under the aforementioned fluences. The depth distribution of damage level and Fe concentration in W with a fluence of 3.87×10^{18} ion m^{-2} is shown in Fig.2 as a representative. The atomic displacement caused by damage appears to be within 300 nm with a peak

located at ~ 70 nm. The peak concentration of injected iron atoms is less than 4×10^{-2} at. %, which allows us to neglect the possible impurity effect from implanted Fe ions.

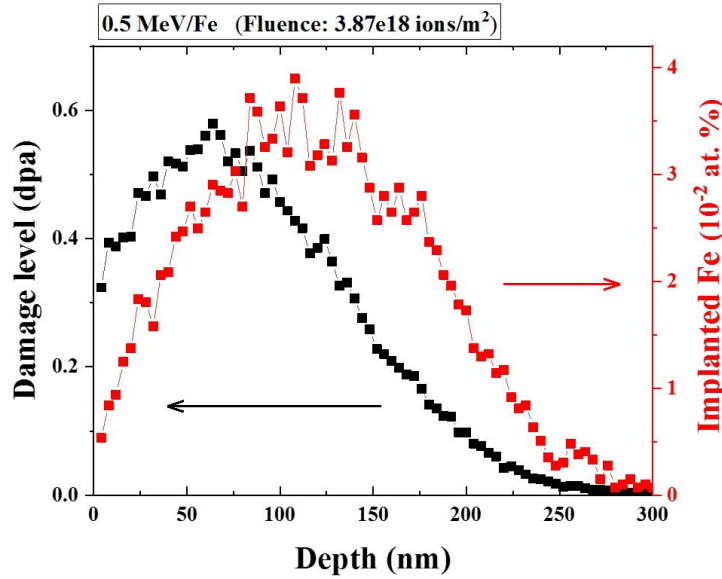


Fig. 2 Depth distribution of damage level & Fe concentration in W irradiated by 0.5 MeV Fe^{10+} ions with a fluence of $3.87 \times 10^{18} m^{-2}$.

Doppler broadening spectroscopy in the positron annihilation technique (PA-DBS) was employed to examine the defect evolution behavior in both damaged & undamaged W and W-Re alloy samples. Positron annihilation technology is based on the detection of gamma photons emitted due to positrons annihilation in materials, so that the information about the electron momentum distribution and defect microstructure in the sample can be extracted. The positron injection was carried out at room temperature using an energy-variable slow positron beam at the institute of high energy physics (IHEP), Chinese Academy of Sciences [21]. Positrons were generated by a ^{22}Na radiation source and the positron energy was continuously adjustable (from 0.5 keV to 20.5 keV). The injection depth (R) of positrons was calculated by the equation: $R = (40/\rho) E^{1.6}$, where ρ is the density of material and E is the energy of injected positrons [22]. The maximum energy of the incident positron (~ 20.5 keV) corresponds to a maximum detection depth of around 250 nm, which fits nicely to the depth of the produced heavy-ion damage shown in Fig. 2. A high-purity Ge detector was used to detect the gamma photons produced in the process of positron annihilation. Positron

annihilation technology is based on the detection of gamma photons emitted due to positrons annihilation in materials, so that the information about the electron momentum distribution and defect microstructure in the sample can be extracted. The gamma ray spans a certain energy range due to the Doppler effect. The PA-DBS measurement from PAT records the energy of gamma rays, with which a Doppler broadening spectrum will be obtained. To analyze the spectrum *S*-parameter and *W*-parameter are proposed, where *S*-parameter defines the ratio of the central area (510.2-511.8 keV) to the whole spectrum area and *W*-parameter defines the ratio of the wing area (513.6-516.9 keV and 505.1-508.4 keV) to the whole spectrum area. With this definition, *S*-parameter describes the positron annihilation with low-momentum valence electrons., and *W*-parameter describes the positron annihilation with high-momentum core electrons. Therefore, *S*-parameter is very sensitive to open volume defects while the *W*-parameter is more sensitive to the chemical environment of the annihilation. An increase of *S*-parameter corresponds to an enhanced volume of vacancy-type defects. (*S*, *W*) plots can distinguish the positron annihilation environment [23]. For a specific bulk, the slope of (*S*, *W*) plot will change as the type of vacancy-defects changes [Appl. Phys. Lett. 64 (1994) 1380].” Usually the (*S*, *W*) plots of positrons annihilated in the similar-type of open-volume defect display linearly. That is, linear distribution of (*S*, *W*) plots implicates the existence of the same type of open-volume defect. In metals, open-volume defect are vacancy-type defects, similar type of open-volume defect corresponds to similar size of vacancy-type defects. Therefore, the similar (different) slope of (*S*, *W*) plots represents the similar (different) kind of vacancy-type defect.[24].

To study the Re effect on the evolution of other type of defects, undamaged W and W-Re alloy samples were simultaneously exposed to D plasma at ~373 K for 68 hours, with an energy of 38 eV/D. The plasma exposure was performed on PlaQ installation in Max-Planck-Institut für Plasmaphysik (IPP), Germany [25]. The ion flux was $8.9 \times 10^{19} \text{ D m}^{-2}\text{s}^{-1}$ and the total fluence was $2.2 \times 10^{25} \text{ D m}^{-2}$. During exposure, the

sample temperature was controlled by a silicon-oil-cooling circuit with a thermocouple integrated in the substrate holder just underneath samples.

After D plasma exposure, surface blistering morphologies were characterized by scanning electron microscopy (SEM) integrated with focused ion beam (FIB) for cross-sectioning. A detailed statistic study was performed for the surface blistering morphology measured by confocal laser scanning microscopy. The grain orientation was examined by electron backscattered diffraction technique (EBSD). The depth distributions of deuterium at the near-surface ($< 8 \mu\text{m}$) were measured by nuclear reaction analysis (NRA) using D- ^3He reaction. The energy of ^3He ion beam was varied in the range of 0.69~4.5 MeV to get data from different depths [26]. The yielded protons and α particles were both collected to derive the deuterium concentration profiles using SIMNRA and NRADC programs [27]. After NRA measurements, the total retained D amount in all plasma-exposed samples was measured by thermal desorption spectroscopy (TDS) starting from a basic pressure of $\sim 1 \times 10^{-6}$ Pa. Samples were heated with a ramp rate of 1 K/s to 1200 K, which is monitored by a thermal couple attached to the sample in the rear side. Release fluxes of D_2 (mass 4) and HD (mass 3) were monitored by a quadrupole mass spectrometer (MKS Micro Vision). D from D_2 and HD were both taken into account for the calculation of D retention. In order to determine the background signal of the TDS system, specimens without exposure to D plasma were measured. The uncertainty of the quadrupole mass spectrometer is $\sim 5\%$ [28]. To get an idea on how much D is released as D_2O and HDO, given the fact that both D_2O and HDO are not calibratable in typical TDS set-ups, we applied the same protocol as proposed in Ref.[29][30] to evaluate the general uncertainty of our TDS measurements. The such evaluated experimental uncertainty is displaced later on in Fig. 11. By comparing the total retained amount of D in different depth from different samples, the evolution of D bulk diffusion was analyzed to further understand the effect of Re on defect evolution in W during D plasma exposure.

3. Results

3.1 Vacancy-type defects evolution during heavy-ion irradiation

Fig. 3 shows the depth distribution of S -parameter in both pure W and W-Re alloy for the Fe ion penetration depth. Before comparing in detail, it should be stressed that the positron annihilation technique provides only qualitative description of vacancy-type defects evolution under heavy-ion irradiation. It cannot provide information on the evolution of other types of defects (e.g. dislocation) [31], but this does not exclude Re effects on such defects evolution. The Re effects on dislocations, for example, will be discussed further below. Moreover, the mechanical polishing induced surface distortions would affect the S -parameter and other measurement results, but since all the samples have experienced the same polishing procedures, such distortion should exert little influence on the conclusion drawn based on the comparison of results due to heavy-ion irradiation and following deuterium plasma exposure.

In Fig.3, the slightly higher S -parameter in the near surface (≤ 50 nm) is supposed to be influenced by surface effects when the positron incident energy is low[32]. Therefore, the S -parameter within this topmost surface could be neglected. From a depth of ~ 50 nm on, the S -parameter in undamaged W (marked as W-0 dpa) is around 0.435. The undamaged W-Re alloy (marked as WRe-0 dpa) shows basically a similar value and trend of S -parameter as in undamaged W. In the depth range of 50~200 nm, the value of S -parameter in undamaged samples is basically stable, and this stable value indicates the lattice condition in pristine materials.

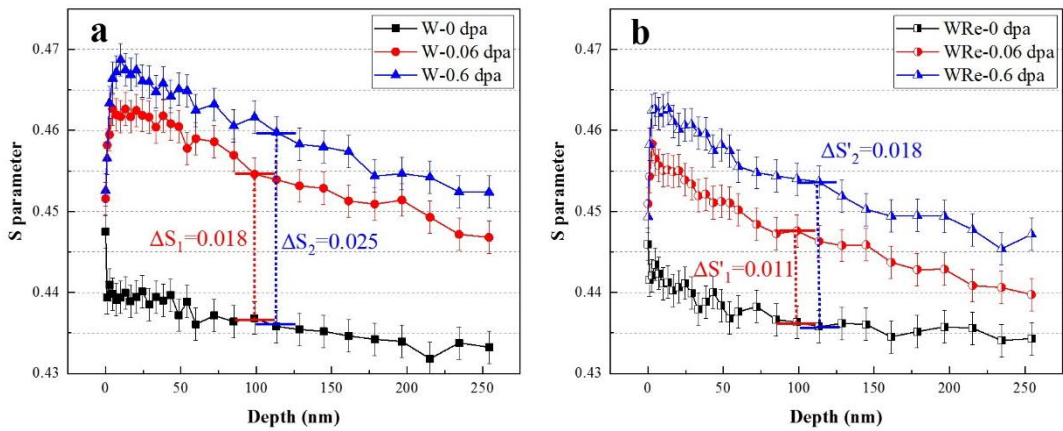


Fig. 3 Depth distribution of S -parameter in various W (a) and W-Re alloy (b) samples.

There is a significant increase of the S -parameter on damaged W compared with undamaged W. Values of the S -parameter at the depth around 100 nm were chosen for quantitative comparison. These values are considered representative for the overall difference between samples since the curves in both sub-figures show in general very similar trends. The S -parameter of W with damage level of 0.06 dpa is 0.018 higher than the S -parameter of undamaged W. W with damage level of 0.6 dpa has an even higher S -parameter, which is 0.025 higher than undamaged W. Similarly, the values of the S parameter in WRe-0.06 dpa and WRe-0.6 dpa are 0.011 and 0.018 higher than that of undamaged W-Re alloy, respectively. These increased S -parameters suggest that plenty of vacancy-type defects were induced by heavy-ion irradiation. To compare W and W-Re alloy, it is clear that under the same damage level, the growth rate of S -parameter in damaged W is higher than that in damaged W-Re alloy.

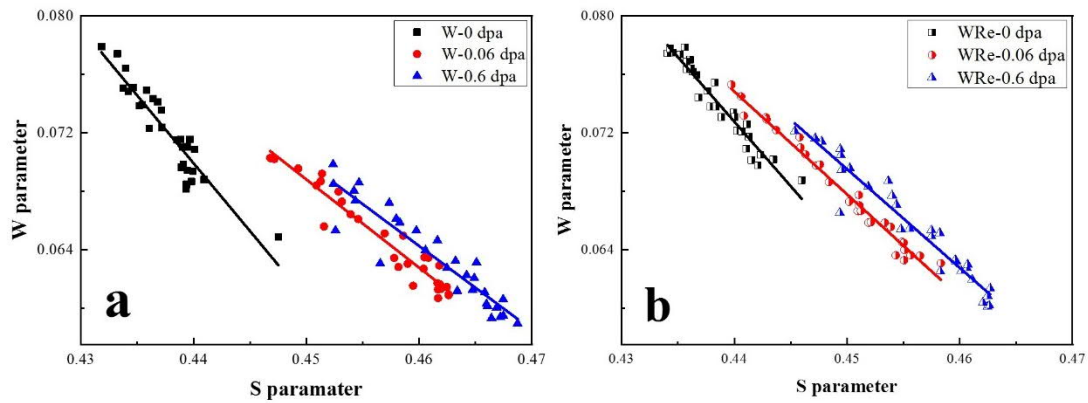


Fig. 4 The plots of W parameter versus S -parameter for W (a) and W-Re alloy (b). Straight lines are the linear fits of the (S , W) plots.

Fig. 4 shows the (S , W) plots of W and W-Re alloy samples. The (S , W) plots generated by the scanning of positron beams with different energies can distinguish different kinds of vacancy-type defects depending on their different slopes. Different slopes of fit lines indicate that positrons were annihilated in different kinds of vacancy-type defects [33]. In Fig. 4 (a), the slope of (S , W) plot of undamaged W is -0.93, while the (S , W) plots of damaged W samples show comparable slopes of -0.60 and -0.57. The obvious difference between (S , W) plot slopes of undamaged W and damaged W reveals that heavy-ion damage caused significant change in the composition of

vacancy-type defects. Normally, the vacancy-type defects in undamaged W are dominated by monovacancy. After heavy-ion irradiation, both S -parameter and the (S , W) slope increase, which indicates much more other kinds of vacancy-type defects, such as divacancies, vacancy clusters, and so on [23] were introduced during irradiation. In Fig. 4 (b), (S , W) plot the slopes of undamaged W-Re alloy and W-Re alloys with damage level of 0.06 dpa & 0.6 dpa are -0.88, -0.70 and -0.68, respectively. Being also with different (S , W) slopes for undamaged with respect to damaged samples, the W-Re alloy shows less significant change of the slope compared with W materials. This may already point to the Re effect on the evolution behavior of vacancy-type defects: [the presence of Re](#) might inhibit the migration and clustering of vacancies. As a result, the vacancy-type defects in W-Re alloy samples do not increase as significant in volume as in W materials.

3.2 Defects evolution under D plasma exposure

3.2.1 Blistering morphology

To further reveal Re influence on the evolution of other type of defects, e.g., dislocations, grain boundaries, etc., we now turn to compare the surface blistering morphology and the D retention behavior in the samples after D plasma exposure. To get a general impression, the grain orientation dependence of blistering on both undamaged W and W-Re alloy samples were observed firstly, as shown in Fig. 5 with the inverse pole figure (IPF) coloring image incorporated. Blisters in both W and W-Re alloy samples are shown preferably in grains with nearly (111) surface orientation, while for grains with near (100) orientation almost no blisters were found. This phenomenon is consistent with the results reported in many publications (e.g., Ref. [34][35]). The surface layer is easier to be deformed vertically when the surface orientation is near (111), since the slip direction of dislocations in bcc metals is the [111] direction [34][35]. The similar grain orientation dependence in W and W-Re alloy indicates little influence from Re alloying on the bcc lattice structure in the matrix.

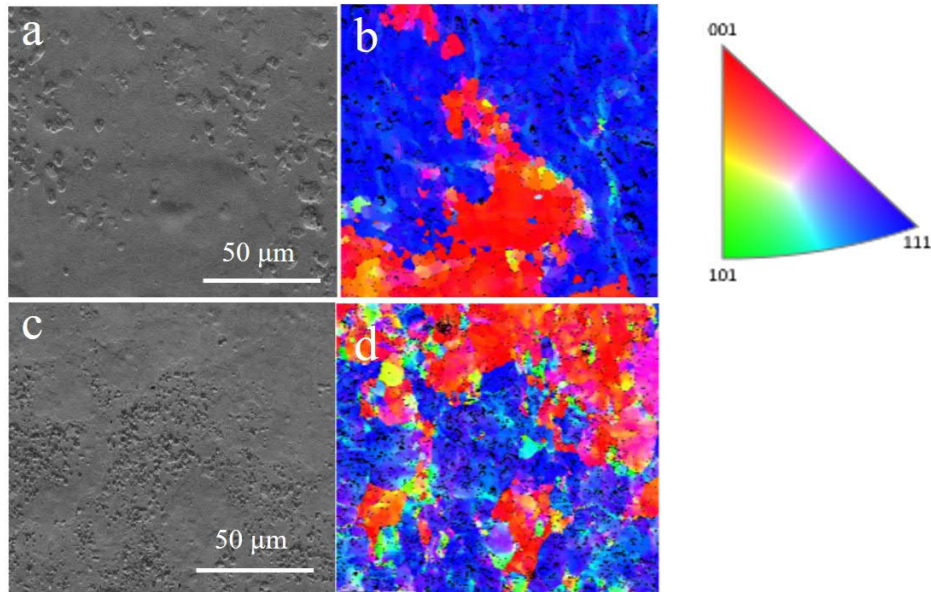


Fig. 5 Surface morphology and corresponding surface orientation IPF map on W (a, b) and W-Re alloy (c, d).

As can be already seen in Fig. 5, the blistering morphology exhibits different size distribution for W and W-Re alloy samples, although its grain orientation dependence is similar in both samples. To acquire more detailed information on the observed blisters, a statistical study on the size distribution of blistering was made from a total evaluated area of $225 \times 225 \mu\text{m}^2$ using confocal laser scanning microscope. The results are shown in Fig. 6 and Table. 1.

In general, blisters from W surface are larger and show broader size distribution than those from W-Re alloy samples. The most frequent blister size from the W-Re alloy sample is less than $1 \mu\text{m}$, while it is $2 \mu\text{m}$ for the W sample. The blister size on the surface of W ranges from 0.5 to $13 \mu\text{m}$ in diameter, with an average value of $2.6 \mu\text{m}$. The average blister sizes on the surface of W-Re alloy is $1.3 \mu\text{m}$. Considering the size distribution of W grains in the matrix (1 - $5 \mu\text{m}$) and the grain orientation dependence, we speculate that the blisters in the W sample are inter-granular while in W-Re alloy most of them are intra-granular blisters. To further confirm this speculation, SEM images with larger magnification are shown in Fig. 7 and Fig. 8.

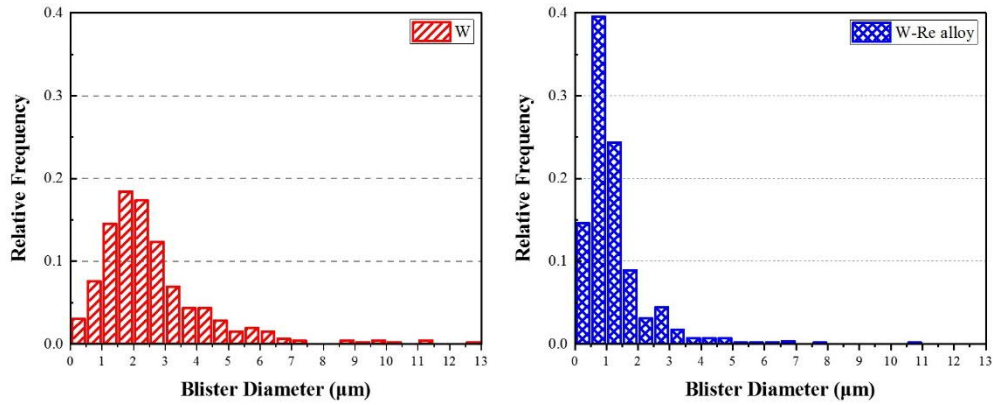


Fig. 6 Blister-size distributions on the surface of W and W-Re alloy after exposure to low energy D plasma.

Table 1. The statistical data of the blister-size distributions for W and W-Re alloy exposed to D plasma

Samples	Average blister size (µm)	Areal density (10 ³ blister/mm ²)	Fraction of surface coverage (%)
W	2.6	9.1	7.2
W-Re alloy	1.3	46.1	9.5

After the D plasma exposure, plenty of blisters appear on all sample surfaces with the abovementioned dependence on grain orientation (see Fig. 7). The SEM images basically confirm the information from the statistical study shown in Table 1. Also, it can be seen in both Fig. 6 and Fig. 7 that the relative frequency of small size blisters ($\leq 1 \mu\text{m}$) on the surface of W-Re alloy is higher than that on W. Presently, we extracted some important aspects of blistering (such as areal density, fraction of surface coverage, etc.) based on the statistical analysis of larger area (i.e., $225 \times 225 \mu\text{m}^2$). The acquired

areal density of blisters is much larger in W-Re alloy than in W samples, which compensates the much smaller sizes of blisters on W-Re alloy and finally leads to a comparable fraction of surface area to W sample (see Table 1). Such information turns out to be very important for the discussion on blistering effect on the bulk diffusion of D. The combined interaction between the inward D diffusion and blistering will be discussed in Sec. 4.3.

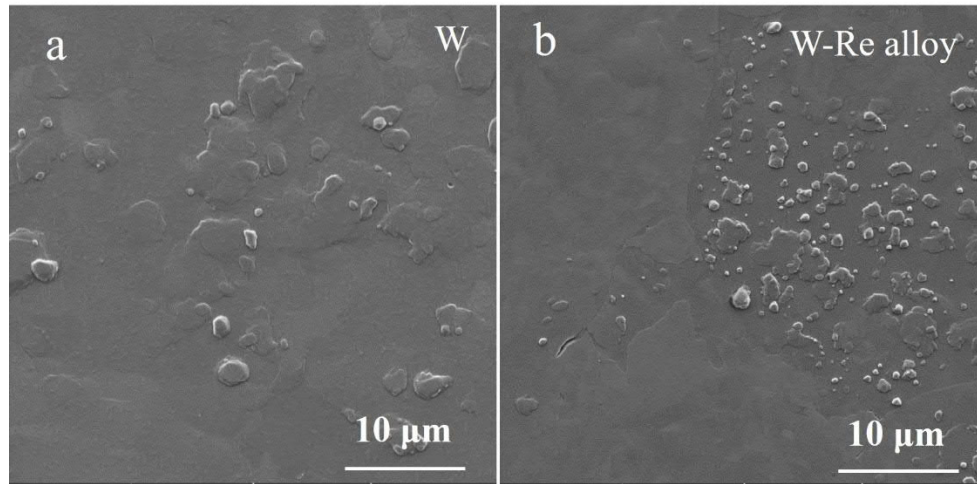


Fig. 7 Surface morphology of samples after D plasma exposure: (a) W; (b) W-Re alloy.

In Fig. 8, some examples of blisters on both W and W-Re alloy samples after D exposure were cut with FIB integrated into SEM. It is reasonable for us to take the deepest point of the cavities as the nucleation point for the blisters. Such depths and the corresponding diameters of blisters were measured and marked in the pictures. The nucleation points of cavities in W are beyond 1 μm and located at grain boundaries. With larger nucleation depth, the blister sizes are also larger, demonstrating the positively correlated dependence. In W-Re alloy, however, cavities exhibit intra-granular characteristic and their nucleation depths are below 1 μm. These cross-sections further confirm the conclusion made above on the blistering morphology: blisters in pure W are inter-granular while in W-Re alloy are dominated by intra-granular ones with smaller cavity depth.

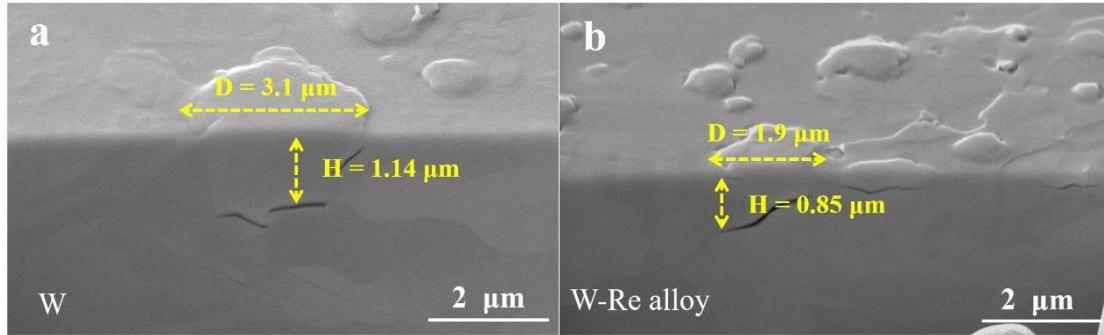


Fig. 8 Cross-section of blister on samples after D exposure: (a) W; (b) W-Re.

3.2.2 D retention and thermal desorption

Fig. 9 exhibits the D depth distribution profiles in W and W-Re alloy after D exposure measured by NRA for an information depth of $\sim 8 \mu\text{m}$. In general, D retention in W-Re alloy is significantly higher than that in W in the depth range of 0-1.5 μm , but the opposite trend appears in the depth range of 1.5-8 μm (Fig. 9b). A closer look at the two D depth profiles yields a surface peak with concentration of a few percent and with layer thickness of a few nanometers for both samples. With the applied bias voltage during plasma exposure being comparable to the critical value for the formation of deuterium super-saturated surface layer [36], the present surface peaks are also attributed to the super-saturation. Beyond this supersaturated surface layer, D concentration in both samples first decreases sharply and then rise again, followed by a gradual decrease towards the deep bulk. Such a ‘bump’ is a typical D concentration profile induced by blistering during plasma exposure. Cavities formed due to blistering can store quite some amount of D_2 gas [37], their propagation will also create new defects acting as traps for D [38]. This gives rise to the bump shape of the D profile. The sharp decrease is attributed to the degassing behavior from the surface. Quite some cavities were found to be open to the surface, which led to the release of initially stored D_2 gas in the cavities and also D trapped at defects in the vicinity of the open crack. The rise of D concentration to higher level in W-Re alloy than in W may be attributed to the following reasons: i) an enhanced D trapping by the alloying element Re acting

as impurity in the W matrix, and ii) more defects have been created in the blister cap layer of W-Re alloy than the W sample. Presently, we cannot distinguish which of the two is the dominant factor determining the higher D concentration at the rise.

As can be seen from Fig. 9b, the peak D concentration of W sample ranges from the depth of 1 μm to 2.1 μm , while it ranges from 0.1 to 0.8 μm in W-Re alloy. Comparing with the results of surface morphology in section 3.2.1, it can be suggested that the peak D concentration comes from the large amount of D retained in the cracks below the blisters. Blisters on the surface of W are larger and the nucleation points are deeper, so the D retention peak appears at a depth beyond 1 μm . W-Re alloy sample has smaller blisters and shallower nucleation points, so the peak D retention occurs within 1 μm . The above facts further confirmed that there is a close relationship between surface blistering and inward D diffusion.

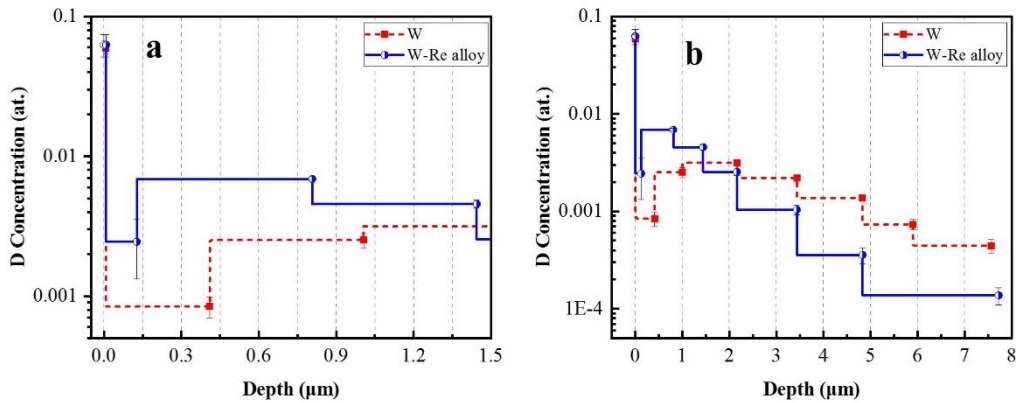


Fig. 9 Deuterium depth profiles in W and W-Re alloy samples: a) enlarged profiles within 1.5 μm ; b) within the whole NRA information depth of $\sim 8 \mu\text{m}$.

Fig. 10 shows the TDS spectra of the two samples after exposure to D plasma. D desorption of both samples starts at the temperature around 370 K – the sample temperature during D plasma exposure. Generally speaking, both D_2 release spectra have two major desorption peaks. However, it yields very different desorption behavior of the retained D: the lower desorption peak of the W sample (~ 530 K) is located at a temperature slightly higher than the larger desorption peak of the W-Re alloy sample (~ 510 K). The second desorption peak of the W sample is located at ~ 680 K with much

higher intensity than its first one. D retention in both samples are obviously dominated by the defects with higher de-trapping energies. Since Re can suppress the mobility of interstitial W atoms and in turn vacancy clustering, it is reasonable to postulate that vacancy clusters in pure W materials are either with larger size or higher density. With larger size, the binding between D and the vacancy cluster are stronger and hence requiring higher de-trapping energy (i.e., higher temperature). More evidences are required to further demonstrate this proposal, which is on-going.

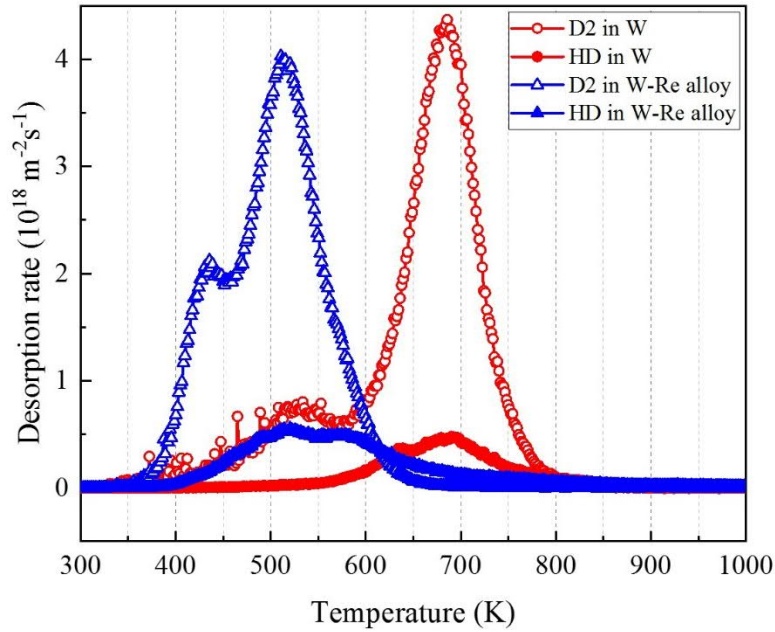


Fig. 10 TDS spectra of W (a) and W-Re alloy (b) samples after D plasma exposure.

As mentioned above, the 8 μm NRA information depth is divided into 2 different regions (0-1.5 μm and 1.5-8 μm). Together with the total retained D amount in the whole sample measured by TDS, the retained D amount at different depths of the samples by integrating the NRA profile to different depth is shown in Fig. 11. The retained D amount beyond 8 μm is acquired by subtracting the NRA total D amount from that measured by TDS. Within the experimental uncertainty, the two samples show almost the same amount of retained D measured by both NRA and TDS techniques. It seems that the Re alloying does not change the D retention in the sample. However, one should note the very different composition of the bars representing the

D depth distribution. In W sample, about 50% D was retained in the depth of 1.5~8 μm , while in W-Re alloy samples, about 50% D was retained in the depth of 0~1.5 μm . Beyond 8 μm both samples show also comparable amount of retained D. As will be discussed in Sec. 4.3, the different D distribution in W and W-Re alloy sample is attributed to the interaction between blister population and the D bulk diffusion during plasma exposure.

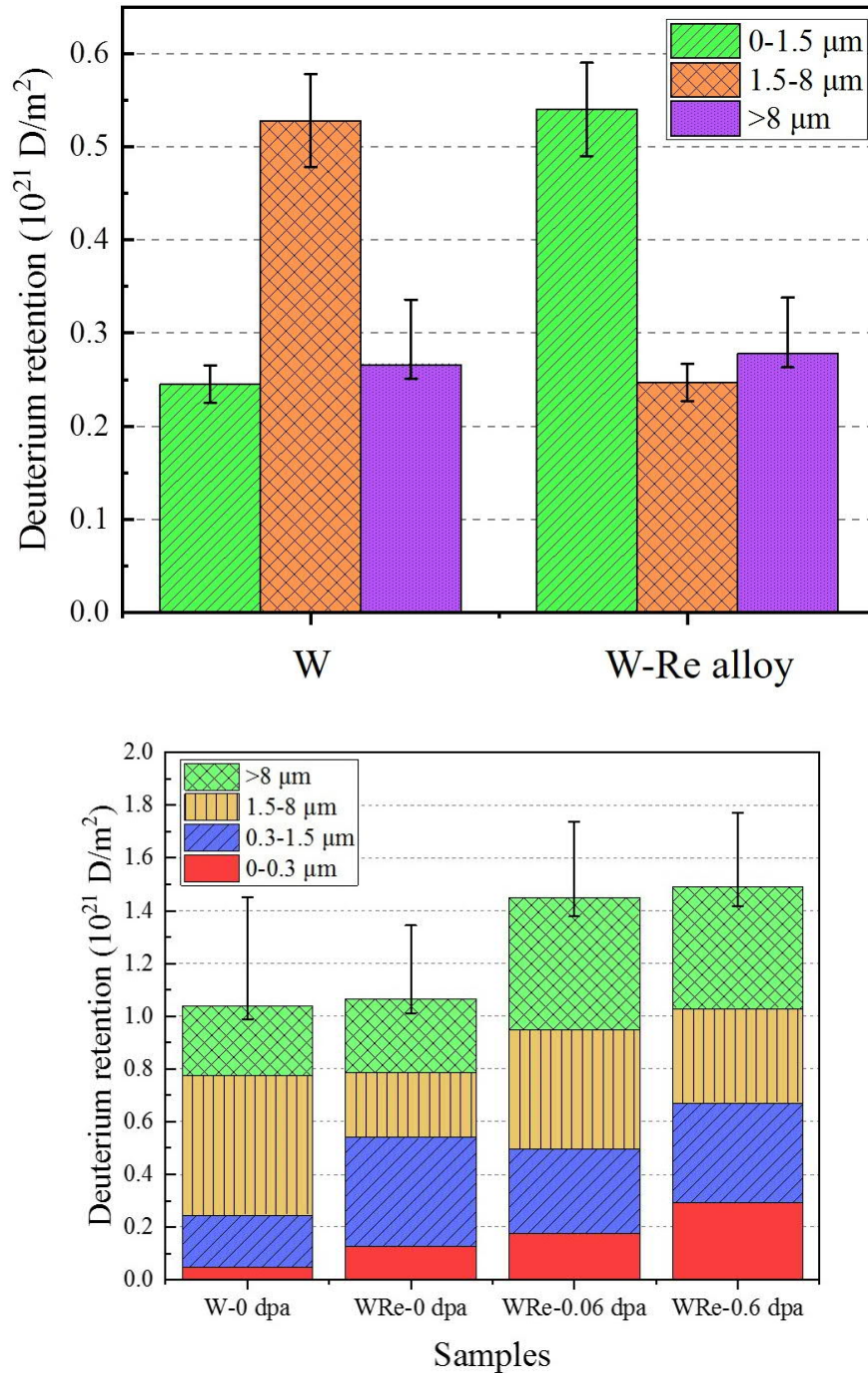


Fig. 11 D retention in W and W-Re alloy measured by NRA and TDS techniques.

4. Discussion

4.1 Re in W matrix: alloying vs transmutation

Before discussing the experimental results, it is wise to discuss the similarity and difference between the presently applied W-Re alloy sample and the neutron-irradiated W components in the future fusion devices. As is well known, Re will grow into W gradually via transmutation in the future fusion devices and a final 5 at. % Re concentration may have to accumulate over a period of several years. During this period, the materials are exposed not only to neutron irradiation but also to intensive heat loads and particle fluxes. It is highly probable that some synergistic processes are active at such extreme circumstances, which are extremely challenging to be addressed experimentally. The present work, therefore, serves as a step to disentangle the synergy by alloying 5% Re directly into tungsten matrix and focusing on the Re effect on defect evolution.

The first question along this motivation is whether the distribution of Re in the W matrix is different or not. The present W-5Re alloy samples are produced via milling/sintering and hot-rolling. Additional EDX scanning has confirmed that Re distribution in W matrix are relatively uniform, no obvious inhomogeneity in terms of Re precipitates due to agglomeration or segregation were found in the sample. However, since EDX is not with atomistic resolution, what can be sure is that Re is not uniformly distributed at the atomistic scale in the present sample. While for W materials accumulating enough neutron irradiation, Re produced via transmutation reaction should initially distribute uniformly at the atomic scale. However, as mentioned above, other conditions (e.g., temperature gradient, irradiation-induced strain, etc.) should be highly probable causing significant redistribution of Re in the W matrix via agglomeration or segregation. Such redistribution, however, is expected to be proceeded towards material with higher similarity to the presently applied W-Re alloy samples.

It is also noted that the neutron-irradiated W materials are also highly damaged, i.e., with very high defect density in accompany with the distribution of transmuted Re. While our hot-rolled materials after annealing should not exhibit very high density of intrinsic defects. Since defect density will exert great influence on the mechanical property of the materials, we postulate that the blistering morphology due to D plasma exposure may in turn be very different for the present materials compared with W after long exposure to fusion neutron irradiation.

4.2 Effect of Re on defects evolution in W

The clearly higher growth of S -parameter in rolled W than W-Re alloy samples by heavy-ion irradiation (Fig. 3) suggests a higher density of vacancy-type defects in the former than the latter material under the same irradiation process. This is explained as follows. The presence of Re substitutional atoms will lead to the formation of W-Re mixed dumbbells with positive binding energies [39][40]. Such W-Re dumbbells require a much higher energy for migration in comparison with W self-interstitials. In other words, Re atoms can suppress the mobility of interstitial W atoms produced during irradiation. Since vacancies are supposed to be immobile and their movements are proceeded via interstitial atoms, the Re-suppressed W interstitial mobility will lead to a lower density of vacancy-type defects.

The same explanation may also apply to the more distinct change of vacancy-type defect compositions in W as compared with W-Re alloy due to damage, as indicated by the (S, W) plots shown in Fig. 4. It is believed that the vacancy-type defects are composed mainly by single vacancies in the as-delivered samples [41]. After heavy-ion irradiation, divacancies or vacancy clusters with even larger size seem to be the main composition formed in pure W samples. However, in the W-Re alloy heavy-ion irradiation does not seem to change significantly the composition of vacancy-type defects. This suggests that the presence of Re might inhibit the migration and clustering of vacancies.

For defects beyond the damage zone, focus is set on dislocations being proposed as the nucleation sites for in-grain cracking/blistering. As demonstrated in Ref. [10][11], Re can suppress the mobility of dislocations in W matrix, i.e., dislocations are pinned or at least dragged by Re during moving. Under the same irradiation condition, pinned dislocations are inclined to form crack nucleation. This is vividly demonstrated by our experiments. W-Re alloy shows mostly in-grain blistering/cracking while almost all cavities in W sample are along grain boundaries. Obviously, dislocations in the W-Re alloy can be initiated for crack nucleation but not in W. Similar results have also been reported in Ref. [14] by Alimov *et al.*, where blisters on W-Re alloy are smaller and denser than those on the surface of W. Although in-grain cracking was also observed in the undamaged W samples in Ref. [14], being attributed to the applied high-flux plasma exposure, the larger blister sizes and cavity depth still back the above-proposed mechanism on pinned dislocations by Re atoms. In the present work, we applied low-flux D plasma exposure aiming at a clear comparison between W-Re alloy and pure W samples: in-grain cracking was only observed in the former but not in the latter sample. The much denser blistering in the W-Re alloy sample may be explained by the newly created dislocations during the propagation of in-grain cracks [42], which could act as new nucleation sites for cracks at higher D fluence. Another possibility is that, Re as an impurity element may act as a nucleation point of dislocations in W. We cannot exclude the possibility that the initial dislocation density in the grains is already higher than that in pure W materials after similar production processes.

4.3 Effect of Re on D retention in W

An interesting fact relevant to the interaction between blister population and D bulk diffusion relies on the comparison on the D depth distribution between W and W-Re alloy samples (see Fig. 9&11). The total retained amounts of D in both samples are comparable but with very different concentration profile at corresponding depth. For example, the D retention in the first 1.5 μm (i.e., above the blistering depth) is almost doubled in W-Re sample as compared with the W sample. While from 1.5-8 μm , D

retention is doubled in the W sample compared with that in the W-Re alloy sample. Blistering plays actually two-fold role for the present situation. On one hand, blistering will create new defects in the cap layer (i.e., $\leq 1.5 \mu\text{m}$) during crack propagation and in turn enhance the final D retention. On the other hand, the formed cavities will block D diffusion towards the larger depth. Although cavities will store D_2 gas, they were mostly found to be open to surface and in turn reduce the D retention. Presently, we are not sure if the doubled D amount in the first $1.5 \mu\text{m}$ of the W-Re alloy sample is dominated by the newly created defects from blistering or by the presence of Re as impurity atoms. However, what can be clearly seen is the more significant blocking effect of the cavities on D bulk diffusion in the W-Re sample, as also supported by the statistical information on the fraction of surface coverage by blisters listed in Table 1. The stronger suppression of D bulk diffusion finally led to much lower D retention in the depth from 1.5 to $8 \mu\text{m}$ in the W-Re sample. Beyond the $8\text{-}\mu\text{m}$ NRA information depth, although the retained D amount is comparable for W and W-Re sample, one cannot simply draw any conclusion on their comparable trap density in the bulk. With different retarding effect on the D diffusion towards the deep bulk, the filling of D at bulk defects may also differ from each other. An even gentler D plasma exposure (e.g., floating potential and higher temperature) may be able to distinguish whether Re itself can be the dominant contributor to D retention in the bulk.

5. Conclusion

To study the influence of the transmutation element Re on defect evolution behaviour in the W, W and W-5Re alloy were exposed to Fe ion beam and D plasma. Reflected by PA-DBS, Re alloying has been demonstrated to suppress the mobility of W interstitials and in turn the clustering behaviour of vacancies created during heavy-ion damaging. Finally, the increase of vacancy-type defects in damaged W is more significant than that in damaged W-Re alloy. After exposure to D plasma, numerous blisters with strong orientation dependence appear on the surface of materials. Blisters on the surface of W-Re alloy are smaller and denser than those on W surfaces, reveals

the pinning effect of Re atoms on dislocations, which facilitates in-grain cracking formation and affects the bulk diffusion of D. Furthermore, the interaction of blister population and the D bulk diffusion has also been discussed in this paper, which gives rise to the comparable total amount of retained D but with very different depth distribution.

Based on a series of experiments, the present work demonstrates the important role of Re on the defect evolution in irradiated W. However, as discussed in Sec. 4.1, we would like to stress the care needed to be taken when extrapolating the present conclusion for the W components under neutron irradiation-induced transmutation in future fusion devices, where the damage zone by neutron is not limited only at the topmost surface but will cover the whole sample thickness. The here-observed interaction between blister population and D bulk diffusion may behave differently in neutron-irradiated W components.

Acknowledgement

This work is supported by the National Natural Science Foundation of China with Grant No. 11905003, No. 12075020 and No. 11905140.

References

- [1] Ueda Y, Coenen J W, De Temmerman G, Doerner R P, Linke J, Philipps V and Tsitron E 2014 Research status and issues of tungsten plasma facing materials for ITER and beyond *Fusion Eng. Des.* **89** 901–6
- [2] Rieth M, Dudarev S L, Gonzalez De Vicente S M, Aktaa J, Ahlgren T, Antusch S, Armstrong D E J, Balden M, Baluc N, Barthe M F, Basuki W W, Battabyal M, Becquart C S, Blagoeva D, Boldyryeva H, Brinkmann J, Celino M, Ciupinski L, Correia J B, De Backer A, Domain C, Gaganidze E, Garcia-Rosales C, Gibson J, Gilbert M R, Giusepponi S, Gludovatz B, Greuner H, Heinola K, Hentschen T, Hoffmann A, Holstein N, Koch F, Krauss W, Li H, Lindig S, Linke J, Linsmeier C, Lopez-Ruiz P, Maier H, Matejicek J, Mishra

- T P, Muhammed M, Mu??oz A, Muzyk M, Nordlund K, Nguyen-Manh D, Opschoor J, Ord??s N, Palacios T, Pintsuk G, Pippan R, Reiser J, Riesch J, Roberts S G, Romaner L, Rosi??ski M, Sanchez M, Schulmeyer W, Traxler H, Ure??a A, Van Der Laan J G, Veleva L, Wahlberg S, Walter M, Weber T, Weitkamp T, Wurster S, Yar M A, You J H and Zivelonghi A 2013 Recent progress in research on tungsten materials for nuclear fusion applications in Europe *J. Nucl. Mater.* **432** 482–500
- [3] Yin H, Wang J, Guo W, Cheng L, Yuan Y and Lu G 2019 Recent studies of tungsten-based plasma-facing materials in the linear plasma device STEP *Tungsten* **1** 132–40
- [4] Knaster J, Moeslang A and Muroga T 2016 Materials research for fusion *Nat. Phys.* **12** 424–34
- [5] Gilbert M R and Sublet J-C 2011 Neutron-induced transmutation effects in W and W-alloys in a fusion environment *Nucl. Fusion* **51** 043005
- [6] Wang Z, Wang J, Yuan Y, Cheng L, Qin S-Y, Kreter A and Lu G-H 2019 Effects of tantalum alloying on surface morphology and deuterium retention in tungsten exposed to deuterium plasma *J. Nucl. Mater.* **522** 80–5
- [7] Wang J, Cheng L, Yuan Y, Qin S-Y, Arshad K, Guo W-G, Wang Z, Zhou Z-J and Lu G-H 2018 Blistering behavior and deuterium retention in tungsten vanadium alloys exposed to deuterium plasma in the linear plasma device STEP *J. Nucl. Mater.* **500** 366–72
- [8] Gao L, Von Toussaint U, Jacob W, Balden M and Manhard A 2014 Suppression of hydrogen-induced blistering of tungsten by pre-irradiation at low temperature *Nucl. Fusion* **54**
- [9] Bauer J, Schwarz-Selinger T, Schmid K, Balden M, Manhard A and Von Toussaint U 2017 Influence of near-surface blisters on deuterium transport in tungsten *Nucl. Fusion* **57** aa7212

- [10] Yi X, Jenkins M L, Hattar K, Edmondson P D and Roberts S G 2015 Characterisation of radiation damage in W and W-based alloys from 2 MeV self-ion near-bulk implantations *Acta Mater.* **92** 163–77
- [11] Yi X, Jenkins M L, Kirk M A, Zhou Z and Roberts S G 2016 In-situ TEM studies of 150 keV W⁺ion irradiated W and W-alloys: Damage production and microstructural evolution *Acta Mater.* **112** 105–20
- [12] Wang S, Zhu X, Cheng L, Guo W, Liu M, Xu C, Yuan Y, Fu E, Cao X Z and Lu G H 2018 Effect of heavy ion pre-irradiation on blistering and deuterium retention in tungsten exposed to high-fluence deuterium plasma *J. Nucl. Mater.* **508** 395–402
- [13] Zhu X L, Zhang Y, Kreter A, Shi L Q, Yuan Y, Cheng L, Linsmeier C and Lu G H 2018 Aggravated blistering and increased deuterium retention in iron-damaged tungsten after exposure to deuterium plasma with various surface temperatures *Nucl. Fusion* **58**
- [14] Hasegawa A, Fukuda M, Yabuuchi K and Nogami S 2016 Neutron irradiation effects on the microstructural development of tungsten and tungsten alloys *J. Nucl. Mater.* **471** 175–83
- [15] Golubeva A V., Mayer M, Roth J, Kurnaev V A and Ogorodnikova O V. 2007 Deuterium retention in rhenium-doped tungsten *J. Nucl. Mater.* **363–365** 893–7
- [16] Alimov V K, Hatano Y, Sugiyama K, Balden M, Oyaidzu M, Akamaru S, Tada K, Kurishita H, Hayashi T and Matsuyama M 2014 Surface morphology and deuterium retention in tungsten and tungsten-rhenium alloy exposed to low-energy, high flux D plasma *J. Nucl. Mater.* **454** 136–41
- [17] Ma F F, Wang W, Li Y H, Zhou H B and Lu G H 2018 Towards understanding the influence of Re on H dissolution and retention in W by investigating the interaction between dispersed/aggregated-Re and H *Nucl. Fusion* **58**

- [18] Zhou X 2016 The heavy ion research facility in Lanzhou *Nucl. Phys. News* **26** 4–9
- [19] Ziegler J F, Ziegler M D and Biersack J P 2010 SRIM - The stopping and range of ions in matter (2010) *Nucl. Instruments Methods Phys. Res. Sect. B Beam Interact. with Mater. Atoms* **268** 1818–23
- [20] Kai Nordlund, Andrea E. Sand, Granberg F, J. Zinkle S, Stoller R, S. Averback R, Suzudo T, Malerba L, Banhart F, Weber W J, Willaime F and , Sergei Dudarev D S 2015 Primary Radiation Damage in Materials *OCDE / Nucl. Sci. NEA/NSC/DOC(2015)9*
- [21] Bao-Yi W, Yan-Yun M, Ping W, Xing-Zhong C, Xiu-Bo Q, Zhe Z, Run-Sheng Y and Long W 2008 Development and application of the intense slow positron beam at IHEP *Chinese Phys. C* **32** 156–9
- [22] Saarinen K, Hautojärvi P, Vehanen A, Krause R and Dlubek G 1989 Shallow positron traps in GaAs *Phys. Rev. B* **39** 5287–96
- [23] Zhu X L, Zhang Y, Cheng L, Yuan Y, De Temmerman G, Wang B Y, Cao X Z and Lu G H 2016 Deuterium occupation of vacancy-type defects in argon-damaged tungsten exposed to high flux and low energy deuterium plasma *Nucl. Fusion* **56** 36010
- [24] Liskay L, Corbel C, Baroux L, Hautojärvi P, Bayhan M, Brinkman A W and Tatarenko S 1994 Positron trapping at divacancies in thin polycrystalline CdTe films deposited on glass *Appl. Phys. Lett.* **64** 1380–2
- [25] Manhard A, Schwarz-Selinger T and Jacob W 2011 Quantification of the deuterium ion fluxes from a plasma source *Plasma Sources Sci. Technol.* **20** 015010
- [26] Mayer M, Gauthier E, Sugiyama K and von Toussaint U 2009 Quantitative depth profiling of deuterium up to very large depths *Nucl. Instruments Methods Phys. Res. Sect. B Beam Interact. with Mater. Atoms* **267** 506–12

- [27] Schmid K and Von Toussaint U 2012 Statistically sound evaluation of trace element depth profiles by ion beam analysis *Nucl. Instruments Methods Phys. Res. Sect. B Beam Interact. with Mater. Atoms* **281** 64–71
- [28] Qin S, Gao L, Wang J, Jacob W, Yuan Y, Lu G-H and Cheng L 2018 Effect of exposure temperature on deuterium retention and surface blistering of tungsten exposed to sequential nitrogen and deuterium plasma *Nucl. Fusion* **58** 106027
- [29] Salançon E, Dürbeck T, Schwarz-Selinger T, Genoese F and Jacob W 2008 Redeposition of amorphous hydrogenated carbon films during thermal decomposition *J. Nucl. Mater.* **376** 160–8
- [30] Wang P, Jacob W, Gao L, Dürbeck T and Schwarz-Selinger T 2013 Comparing deuterium retention in tungsten films measured by temperature programmed desorption and nuclear reaction analysis *Nucl. Instruments Methods Phys. Res. Sect. B Beam Interact. with Mater. Atoms* **300** 54–61
- [31] Slotte J 2006 Positron annihilation spectroscopy of vacancy complexes in SiGe *Nucl. Instruments Methods Phys. Res. Sect. B Beam Interact. with Mater. Atoms* **253** 130–5
- [32] Zibrov M, Egger W, Heikinheimo J, Mayer M and Tuomisto F 2020 Vacancy cluster growth and thermal recovery in hydrogen-irradiated tungsten *J. Nucl. Mater.* **531** 152017
- [33] Saarinen K, Laine T, Kuisma S, Nissila J, Hautajarvi P, Dobrzynski L, Baranowski J M, Pakula K, Stepniewski R, Wojdak M, Wysmolek A, Suski T, Leszczynski M, Grzegory I and Porowski S 1997 Observation of native Ga vacancies in GaN by positron annihilation *Mater. Res. Soc. Symp. - Proc.* **482** 757–62
- [34] Jia Y Z, De Temmerman G, Luo G N, Xu H Y, Li C, Fu B Q and Liu W 2015 Surface morphology and deuterium retention in tungsten exposed to high flux D plasma at high temperatures *J. Nucl. Mater.* **457** 213–9

- [35] Miyamoto M, Nishijima D, Ueda Y, Doerner R P, Kurishita H, Baldwin M J, Morito S, Ono K and Hanna J 2009 Observations of suppressed retention and blistering for tungsten exposed to deuterium–helium mixture plasmas *Nucl. Fusion* **49** 065035
- [36] Gao L, Jacob W, Von Toussaint U, Manhard A, Balden M, Schmid K and Schwarz-Selinger T 2017 Deuterium supersaturation in low-energy plasma-loaded tungsten surfaces *Nucl. Fusion* **57**
- [37] Balden M, Lindig S, Manhard A and You J H 2011 D₂ gas-filled blisters on deuterium-bombarded tungsten *J. Nucl. Mater.* **414** 69–72
- [38] Cheng L, De Temmerman G, Morgan T W, Schwarz-Selinger T, Yuan Y, Zhou H B, Wang B, Zhang Y and Lu G H 2017 Mitigated blistering and deuterium retention in tungsten exposed to high-flux deuterium-neon mixed plasmas *Nucl. Fusion* **57**
- [39] Suzudo T, Yamaguchi M and Hasegawa A 2014 Stability and mobility of rhenium and osmium in tungsten: First principles study *Model. Simul. Mater. Sci. Eng.* **22**
- [40] Suzudo T, Yamaguchi M and Hasegawa A 2015 Migration of rhenium and osmium interstitials in tungsten *J. Nucl. Mater.* **467** 418–23
- [41] Nambissan P M G and Sen P 1992 Positron annihilation study of the annealing behaviour of alpha induced defects in tungsten *Radiat. Eff. Defects Solids* **124** 215–21
- [42] Guo W, Ge L, Yuan Y, Cheng L and Wang S 2019 001edge dislocation nucleation mechanism of surface blistering in tungsten exposed to deuterium plasma